References for Small Fluorescence Quantum Yields

Mahbobeh Morshedi, Simon L. Zimmermann, David Klaverkamp & Peter Gilch

Suggested Citation:
Morshedi, M., Zimmermann, S., Klaverkamp, D., & Gilch, P. (2024). References for Small Fluorescence Quantum Yields. Journal of Fluorescence, 35(5), 3253–3266. https://doi.org/10.1007/s10895-024-03729-2

Journal of Fluorescence (2025) 35:3253–3266
https://doi.org/10.1007/s10895-024-03729-2

RESEARCH

References for Small Fluorescence Quantum Yields

Mahbobeh Morshedi[1] · **Simon L. Zimmermann**[1] · **David Klaverkamp**[1] · **Peter Gilch**[1]

Received: 14 March 2024 / Accepted: 11 April 2024 / Published online: 15 May 2024

Abstract

Three compounds with fluorescence quantum yields in the range of 10^{-5} to 10^{-4} and emission spectra covering the UV/Vis spectral range are suggested as new references for the determination of small fluorescence quantum yields. The compounds are thymidine (dT) in water, dibenzoylmethane (DBM) in ethanol, and malachite green chloride (MG) in water, representing the blue, green, and red regions of the spectrum, respectively. All compounds are easily handled, photostable, and commercially available. Furthermore, these compounds exhibit a mirror-image symmetry between their absorption and fluorescence spectra. This symmetry, along with closely aligned fluorescence excitation and absorption spectra, confirms that the observed emissions originate from the compounds themselves. The fluorescence quantum yields were determined via a relative approach as well as Strickler-Berg analysis in conjunction with time resolved fluorescence spectroscopy. Within the respective error margins, the two approaches yielded identical results.

Graphical Abstract

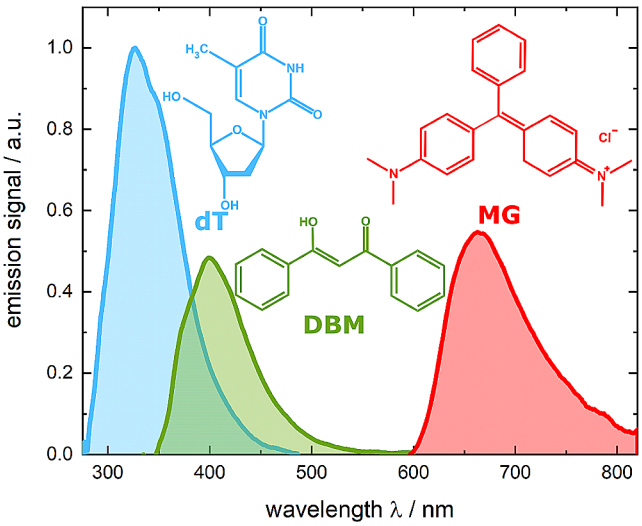

Keywords Fluorescence quantum yield · Time resolved spectroscopy · Strickler-Berg analysis · Thymidine · Dibenzoylmethane · Malachite green chloride

✉ Peter Gilch
gilch@hhu.de

Mahbobeh Morshedi
morshedi@hhu.de

Simon L. Zimmermann
simon.zimmermann@hhu.de

David Klaverkamp
david.klaverkamp@hhu.de

[1] Institut für Physikalische Chemie, Heinrich-Heine-Universität Düsseldorf, Universitätsstr. 1, 40225 Düsseldorf, Germany

Introduction

The fluorescence quantum yield $\Phi_{fl.}$ is a key parameter of molecular chromophores. It is given by the ratio of the number of photons emitted *via* fluorescence to the number of photons absorbed by a chromophore. From this definition, it is immediately clear that the yield $\Phi_{fl.}$ is a crucial figure of merit in fluorescence applications. For instance, optical brighteners [1, 2], ingredients of text markers [3, 4], emitters for organic light-emitting diodes (OLEDs) [5, 6], and fluorescence labels for modern microscopy [7] ought to feature yields $\Phi_{fl.}$ close to one. Furthermore, based on these yields, reliable estimates of lifetimes of primary molecular excitations can be made [8]. This gives important first glimpses on the photophysics and photochemistry of a chromophore and facilitates the planning of time resolved spectroscopy [9]. Additionally, precise determinations of the yield $\Phi_{fl.}$ are essential for the quantitative interpretation of Förster resonance energy transfer (FRET) experiments [10, 11].

It is, thus, no surprise that various techniques to determine these yields have been developed. They can be divided into absolute and relative ones. In absolute calorimetric approaches [12, 13], small temperature increases caused by the illumination of a sample are recorded. The temperature increase is approximately proportional to 1-$\Phi_{fl.}$. Calorimetric determinations can mostly be found in the pre-1990s literature. Nowadays, absolute determinations often make use of integrating spheres [14, 15]. With these spheres, signals proportional to the emitted and absorbed light fluxes are recorded. The ratio of these quantities is approximately equal to the yield $\Phi_{fl.}$. Contrary to the absolute methods, for which not so common set-ups are required, relative determinations rely on a widely-used instrument, namely a fluorescence spectrometer. In a relative determination, the spectrally integrated fluorescence signal of a sample is compared with the respective integral of a suitable reference (cf. Equation (4)) [16, 17]. Often solutions of dye molecules serve as a reference [18]. References based on the Raman scattering of neat solvents have also been reported [19].

Therefore, reference materials with approved and certified fluorescence quantum yields are particularly important for many users of fluorescence methods. According to Brouwer [20], the majority of these reference compounds have high fluorescence quantum yields $\Phi_{fl.}$, commonly exceeding 0.5. Many chromophores exhibit yields $\Phi_{fl.}$ many orders of magnitude smaller. Based on the relation (Eq. (1)) between the yield $\Phi_{fl.}$ and rate constants for the radiative (k_{rad}) as well as the non-radiative decay (k_{nr})

$$\Phi_{fl} = \frac{k_{rad}}{k_{rad} + k_{nr}} \tag{1}$$

a lower boundary for this yield can be estimated. We hereby restrict ourselves to organic chromophores with allowed lowest energy singlet transitions. For such chromophores, the radiative rate constant k_{rad} is of the order of 10^8 s^{-1} [9]. Internal conversion (IC) [21, 22], intersystem crossing (ISC) [21, 23–25], excitation energy (EET) [26] as well as electron transfer (ET) [27, 28], and photochemical transformations [28] can lead to non-radiative decays. The upper limit for rate constants of all of these processes results from nuclear motions [21, 29]. Characteristic frequencies of these motions are the ones of molecular vibrations with values of $\sim 10^{13}$-10^{14} s^{-1} [21, 30]. Thus, molecules with allowed transitions and ultrafast non-radiative decays, i.e., k_{nr}=10^{13}-10^{14} s^{-1}, will exhibit fluorescence quantum yields $\Phi_{fl.}$ of the order of 10^{-6}-10^{-5}. Obviously, for molecules with (partially) forbidden transitions, even smaller values may be found. Fluorescence quantum yields $\Phi_{fl.}$ many orders of magnitude smaller than one were indeed often observed experimentally. DNA and RNA bases, for instance, feature yields of $\sim 10^{-4}$ [31]. Photoreactive molecules like *trans*-azobenzene ($\sim 10^{-7}$ [32]), *cis*-stilbene ($\sim 10^{-5}$ in acetonitrile [33]), and rhodopsin ($\sim 10^{-5}$ [34]) exhibit even smaller yields. Triplet sensitizers like xanthone ($\sim 10^{-4}$ in ethanol [35]) and thioxanthone ($\sim 10^{-5}$ in cyclohexane [36]) are also examples for chromophores with very small yields. These examples emphasize the important role of compounds with small fluorescence quantum yields in diverse fields and underscore the need for establishing new reference materials to precisely quantify these yields. Relative determinations of such small fluorescence quantum yields are hampered by the predominance of references with yields of the order of one. As any quantitative comparison, the relative determination of these yields is facilitated if sample and reference exhibit similar signal strengths [37]. This similarity ensures that the measured fluorescence intensities are within the dynamic range of the instrument, thereby reducing errors associated with instrument sensitivity and signal detection limits [38, 39].

Here, we suggest and characterize three references with yields in the range of 10^{-5}-10^{-4} and emission spectra covering the UV/Vis range. Fluorescence quantum yields $\Phi_{fl.}$ of the compounds were determined with the relative approach as well as utilizing the relation between this yield, the radiative rate constant k_{rad}, and the fluorescence lifetime $\tau_{fl.}$ (Eq. (2)) [8],

$$\Phi_{fl} = k_{rad}\tau_{fl.} \tag{2}$$

The radiative rate constant k_{rad} was retrieved from absorption and fluorescence emission spectra *via* the Strickler-Berg relation (cf. Equations (5) and (6)) [40, 41]. This relation can be applied provided that the same pair of electronic states is involved in the absorption and the emission

process. Furthermore, the Condon approximation must be valid [42]. A mirror-image relationship between absorption and emission spectra is an indicator that these conditions are fulfilled [21]. Thus, molecules not obeying this relation were discarded. The fluorescence lifetime $\tau_{fl.}$ was measured using fluorescence Kerr gating [36, 43]. For the weakly fluorescent samples considered here, signals of impurities might surmount the ones of the nominal sample [44]. Matching absorption and fluorescence excitation spectra indicate that the fluorescence indeed (predominately) stems from the sample and not an impurity. Thus, for all samples this was investigated. In addition to these fundamental criteria, also practical ones were considered. Chromophores and solvents commercially available in high purities were selected. The chemical and photochemical stability of chromophores in the given solvent were also a criterium.

Based on these criteria, the following three chromophore/solvent combinations were identified and characterized. The combinations are thymidine (dT) in water, dibenzoylmethane (DBM) in ethanol, and malachite green chloride (MG) in water (see Fig. 1). In this order, they cover the blue, green, and red regions of the UV/Vis range.

For dT in water, previous determinations yielded a fluorescence quantum yield $\Phi_{\mathrm{fl.}}$ of the order of 10^{-4} [45, 46]. For the other two chromophores, reported lifetimes in the range of 100 fs – 1 ps [47–51] suggested yields of the same magnitude. We will also report on a molecule, namely *N, N*-dimethyl-4-nitroaniline (DpNA), which was discarded as determinations based on the relative approach and the one based on the Strickler-Berg analysis in combination with a lifetime measurement did not match.

Following common practice in fluorescence spectroscopy and for ease of handling, solutions were *not* de-oxygenated. Oxygen quenching should essentially not affect yields $\Phi_{\mathrm{fl.}}$ of the compounds listed in Fig. 1. Assuming diffusion limited oxygen quenching (rate constant $k_q \sim 10^{10}\ \mathrm{M^{-1}\ s^{-1}}$ [9]) and inserting a typical concentration of dissolved oxygen ($[O_2] \sim 10^{-3}\ \mathrm{M}$ [9]), one arrives at a time constant τ_{O_2} for oxygen quenching of the order of 100 ns. This is many orders of magnitude longer than the fluorescence lifetimes $\tau_{fl.}$ measured for the compounds in Fig. 1. Thus, oxygen quenching will not affect their fluorescence lifetimes, and according to Eq. (2), the yield $\Phi_{\mathrm{fl.}}$. However, oxygen quenching may affect the yields of the references employed in the relative determinations. The respective compounds feature fluorescence lifetimes $\tau_{fl.}$ in the 1–10 ns range which is closer to the lifetime τ_{O_2}. To avoid systematic errors, references with reported fluorescence quantum yields for aerated solutions were employed.

Experimental Section

Samples

Thymidine (≥ 99.0%) (CAS ID: 50-89-5), L-tyrosine (≥ 99.8%), and malachite green chloride (≥ 90.0%) (CAS ID: 569-64-2) were purchased from Sigma-Aldrich, dibenzoylmethane (99.01%) (CAS ID: 120-46-7) from BLDpharm, coumarin-1 (99.9%) from Acros Organics, rhodamine 101 from Radiant Dyes Laser & Accessories GmbH, *N, N*-dimethyl-4-nitroaniline (≥ 98%) from Tokyo Chemical Industry, water (HPLC gradient grade) from Fisher Chemical, ethanol (≥ 99.8%) from Sigma-Aldrich, and acetonitrile (HPLC gradient grade) from Chem Solute. All measurements were performed at room temperature (~ 20 °C).

Steady State Measurements

Steady state absorption spectra were recorded using Lambda 19 and 1050 + spectrometers from Perkin Elmer. Fluorescence spectra were measured with a FluoroMax-4 (Horiba Scientific). Spectra were corrected for the spectral sensitivity of the instrument. For all steady state measurements, fused

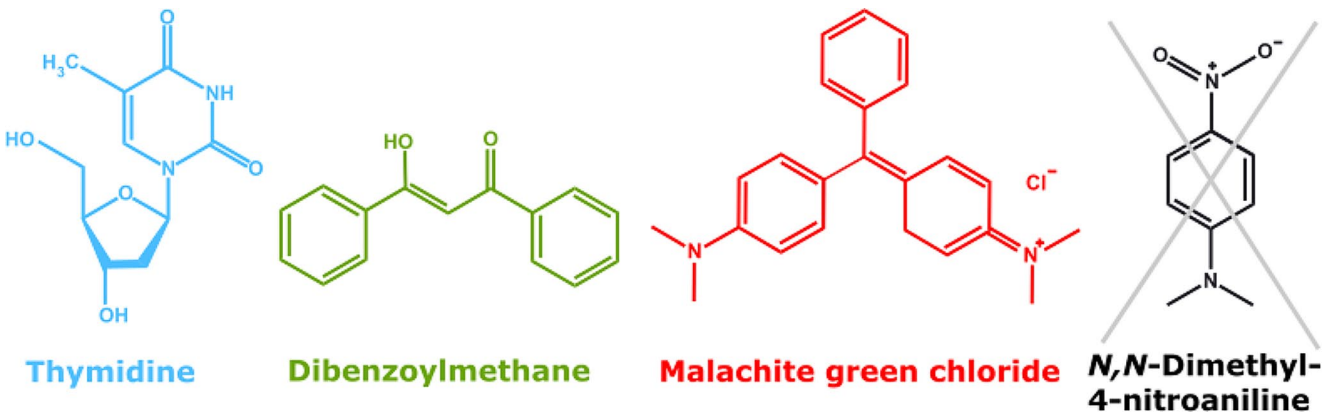

Fig. 1 Chemical structures of thymidine, dibenzoylmethane, malachite green chloride, and *N, N*-dimethyl-4-nitroaniline. The first three molecules plotted in different colors are suggested as references, the last one was discarded

silica cells (from Hellma Analytics) with a path length of 1 cm were employed. In the steady state fluorescence experiments, the sample absorption at the excitation wavelength was kept at ≤ 0.05 for a path length of 1 cm. The small absorption values avoid inner filter effects, i.e. re-absorption of emitted fluorescence, and more importantly ensures a linear scaling between the absorption values and the fluorescence signals. Equation (4) for the relative determination of the fluorescence quantum yields is based on such a scaling. The excitation and emission bandpasses were set to 5 nm for the steady state measurements of all compounds and their respective references. Also, the other settings of the fluorescence spectrometer were identical for samples and references. For the relative determination of the fluorescence quantum yields $\Phi_{fl.}$ of DpNA in acetonitrile, dT in water, DBM in ethanol, and MG in water, the following references were used, respectively: coumarin 1 (C-1) in de-oxygenated water ($\Phi^r_{fl} = 0.055$, note that the value is not significantly affected by oxygen [52]), tyrosine (Ty) in aerated water ($\Phi^r_{fl} = 0.21 \pm 0.01$ [53, 54]), C-1 in de-oxygenated water ($\Phi^r_{fl} = 0.055$ [52]), and rhodamine 101 (Rh 101) in aerated ethanol ($\Phi^r_{fl} = 0.913 \pm 0.046$ [55]). The samples and their respective references were excited at wavelengths close to their absorption maxima, while care was taken to ensure the coverage of their entire emission spectra. The region (~5 nm) around the excitation was avoided. The fluorescence spectra of all samples and their respective references were corrected for the Raman effect by subtracting a suitably scaled spectrum of the solvent, which was recorded under identical conditions.

Time Resolved Fluorescence Measurements

The setup was described in detail elsewhere before [36, 43]. A 1 kHz Ti:Sa laser amplifier system (Coherent Libra) was employed as a pulse source. Its output has a wavelength of 800 nm and a pulse duration of ~100 fs (full width half maximum, FWHM). For the experiment on DpNA in acetonitrile, the excitation wavelength was set to 400 nm. To this end, a portion of the output was converted (in a BBO crystal type I, 29°, 1 mm) to a wavelength of 400 nm by frequency doubling. The beam had an energy per pulse of 1 µJ at the sample location. For the experiments on dT in water and DBM in EtOH, the excitation wavelength was set to 266 nm. To this end, a portion of the output was initially converted (in a BBO crystal type I, 29°, 1 mm) to a wavelength of 400 nm by frequency doubling. Subsequently, the sum frequency was generated (in another BBO crystal, type II, 55.5°, 0.5 mm) to obtain a wavelength of 266 nm from the frequency doubled and the fundamental beam. At the sample location the beam had a diameter of 80 µm (FWHM) and a pulse energy of 1 µJ. For the measurement on MG in water, the excitation wavelength was tuned to 580 nm. To this end, a part of the output was directed to a TOPAS-White non-collinear optical parametric amplifier system. The TOPAS was set to generate pulses peaking at 580 nm with an energy of 0.9 µJ per pulse. The generation of the gate pulses and the operation of the Kerr gate followed the description in ref. [36]. The width of the instrumental response function (IRF), as obtained from Raman scattering of the solvent, was about 250, 270 and 220 fs (FWHM) for 400, 266 and 580 nm excitation light, respectively. For the experiment on DpNA in acetonitrile, the integration time was set to 1 s. Between −5 and 3 ps, the delay time was varied linearly in 60 steps. A total of 13 scans were averaged. For the measurement on dT in water, the integration time for each spectrum was set to 1 s. One scan consisted of 30 equidistant steps between −2 and 3 ps. A total of 14 scans were averaged. For the experiment on DBM in EtOH, the integration time of 2 s was set for each spectrum. In each scan, there were 60 equidistant steps on a linear time axis from −2 to 3 ps. 22 scans were averaged. For the experiment on MG in water, the integration time was set to 1 s. Between −2 and 3 ps, the delay time was varied linearly in 60 steps. A total of 110 scans were averaged. The solutions were circulated through a flow cell (custom made QX, Hellma Analytics) with a path length of 1 mm by a peristaltic pump (REGLO Analog MS-2/8 from ISMATEC®). Signals on solutions of DpNA, dT, DBM, and MG (concentrations of ~0.5 mM, ~1 mM, ~1.3 mM, and ~70 µM, respectively) as well as the neat solvent were recorded. The solvent contributions were subtracted after proper scaling. All time resolved spectra were corrected for the spectral sensitivity of the instrument.

Data Analysis

Time resolved data sets *S(λ, t)* were analyzed globally with a multi-exponential fit function convoluted with the instrumental response function (IRF),

$$S(\lambda, t) = IRF \otimes \sum_{i=1}^{n} S_i(\lambda) \cdot e^{-\frac{t}{\tau_i}}. \quad (3)$$

The fit yields time constants τ_i and decay associated spectra $S_i(\lambda)$ (DAS) [56, 57].

Estimates of Error Margins

For the determination of the statistical error of the yield Φ^{rel}_{fl} (measured by the relative method) and absorption coefficient (ε), multiple independent measurements were performed and the mean value was calculated [58]. The corresponding error margins denote the standard deviations from the mean [58]. The error margins of the reference yield

Φ_{fl}^{r}, if available, were accounted for by error propagation. To determine the error of the radiative rate constant k_{rad}, the error of the respective integrals (see Eq. (5)) entered an error propagation analysis [58]. The error margins in the time constants $\tau_{fl.}$ represent the deviations of the fit from the fluorescence decay data. These margins are determined through exhaustive search error analysis, utilizing the chi-squared (χ^2) statistics to evaluate the quality of the fit by taking into account the correlation among all the fit parameters [59]. The quoted error in the fluorescence quantum yield Φ_{fl}^{SB} (determined through the time resolved method) reflects the propagated errors associated with both the radiative rate constant k_{rad} and the fluorescence lifetime $\tau_{fl.}$.

Results and Discussion

DpNA and its derivative 4-nitroaniline were shown to undergo ultrafast IC with sub-picosecond time constants [60, 61]. Thus, a fluorescence quantum yield $\Phi_{\mathrm{fl.}}$ of the desired magnitude is to be expected. DpNA in acetonitrile exhibits a structureless absorption band lowest in transition energy peaking around 394 nm (see Fig. 2). The fluorescence spectrum peaks at 480 nm. The spectra converted into the transition dipole representation [41, 62] reveal that the mirror-image relationship holds approximately (see Fig. S1 in the Online Resource). The fluorescence excitation spectrum slightly deviates from the properly scaled absorption spectrum shown in Fig. 2b for DpNA in acetonitrile. Its absorption coefficient $\varepsilon_{\max}$ was determined to be $(2.30 \pm 0.08) \times 10^4\ \mathrm{M^{-1}cm^{-1}}$, which is in line with the previously reported value of $2.42 \times 10^4\ \mathrm{M^{-1}cm^{-1}}$ [63]. For the relative determination of the fluorescence quantum yield, DpNA dissolved in acetonitrile was excited close to the maximum at 400 nm (see Fig. 2). The resulting fluorescence signal was compared to the one of C-1 in water. The fluorescence quantum yield based on the relative approach Φ_{fl}^{rel} was computed using Eq. (4) [8]

$$\Phi_{fl}^{rel} = \Phi_{fl}^{r} \frac{\int S_{fl}^{s}(\lambda)\, d\lambda}{\int S_{fl}^{r}(\lambda)\, d\lambda} \frac{A^{r}}{A^{s}} \left(\frac{n^{s}}{n^{r}}\right)^{2}. \tag{4}$$

Here, Φ_{fl}^{r} is the fluorescence quantum yield of the reference, $\int S_{fl}^{s,r}(\lambda)\, d\lambda$ are the spectral integrals of the fluorescence for sample and reference. $A^{s,r} < 0.05$ are the absorptions of sample and reference at the excitation wavelength, and $n^{s,r}$ denotes the refractive index of the solvent of the sample or the reference. Values complied in ref. [52, 64] were inserted. With these inputs, a yield Φ_{fl}^{rel} of $(5.12 \pm 0.06) \times 10^{-5}$ results for DpNA in acetonitrile.

Using the spectra depicted in Fig. 2, a Strickler-Berg analysis was conducted. In this analysis, the radiative rate constant k_{rad} is obtained from spectral integrals (covering a part) of the absorption spectrum and the fluorescence spectrum (Eqs. (5, 6)) [40, 41],

$$k_{rad} = \frac{8\pi \ln(10)\, c_0 n^2}{N_A} \left\langle \tilde{v}^{-3} \right\rangle^{-1} \int \frac{\varepsilon(\tilde{v})\, d\tilde{v}}{\tilde{v}}, \tag{5}$$

$$\left\langle \tilde{v}^{-3} \right\rangle^{-1} = \frac{\int S_{fl}(\tilde{v})\, d\tilde{v}}{\int \tilde{v}^{-3} S_{fl}(\tilde{v})\, d\tilde{v}}. \tag{6}$$

Here, c_0 is the speed of light, n the refractive index of the solvent, and N_A Avogadro´s number. The factor $\left\langle \tilde{v}^{-3} \right\rangle^{-1}$ accounts for the cubic dependence of the spontaneous emission on the wavenumber $\tilde{\nu}$. Its evaluation involves integrals covering the fluorescence spectrum $S_{fl}\left(\tilde{\nu}\right)$ as a function of the wavenumber $\tilde{\nu}$. The fluorescence spectra $S_{fl}^{\lambda}(\lambda)$ were recorded as a function of the wavelength λ and with a constant wavelength bandpass (5 nm). For the conversion to wavenumber axis, the spectrum $S_{fl}^{\lambda}(\lambda)$ was multiplied by the wavelength λ squared, $S_{fl}\left(\tilde{\nu}\right) \sim S_{fl}^{\lambda}(\lambda)\, \lambda^2$ [8]. The molar decadic absorption $\varepsilon(\tilde{v})$ as a function of the wavenumber $\tilde{\nu}$ enters the integral $\int \frac{\varepsilon(\tilde{v}) d\tilde{v}}{\tilde{v}}$. It is crucial that this integral only covers the part of the spectrum $\varepsilon(\tilde{v})$ associated with the transition to the lowest excited singlet state. The respective range is marked in Fig. 2. The respective evaluation affords a radiative rate constant k_{rad} of $(1.72 \pm 0.08) \times 10^8\ \mathrm{s^{-1}}$.

In the fluorescence Kerr gating experiment, a solution of DpNA dissolved in acetonitrile was excited with femtosecond pulses centered at 400 nm (Fig. 3). Time resolved spectra closely match the shape of the steady state one, with a peak around 480 nm. Within one picosecond, almost all the emission signal has vanished (Fig. 3). The experimental results were subject to a global analysis using a single-exponential convoluted with the IRF as a trial function (see Experimental section). The procedure affords a fluorescence lifetime $\tau_{fl.}$ of 590 ± 190 fs. In a previous study a time constant of 630 fs was reported [61]. Multiplying this lifetime with the radiative rate constant determined above results in a fluorescence quantum yield Φ_{fl}^{SB} of $(1.01 \pm 0.3) \times 10^{-4}$ (see Eq. (2)). This value is approximately twice the yield Φ_{fl}^{rel} determined by the relative approach. Due to this discrepancy, DpNA was discarded as a reference.

Semi-empirical quantum chemical computations [66] and transient absorption experiments [61] performed by Ernsting et al. can rationalize this discrepancy. For the closely related molecule 4-nitroaniline, these computations predict an ultrafast (< 100 fs) decrease of the oscillator strength f and thereby the radiative rate constant k_{rad} after photo-excitation. In transient absorption experiments with a time resolution of ~ 50 fs, which compares to ~ 250 fs in the fluorescence experiments reported here, such an ultrafast

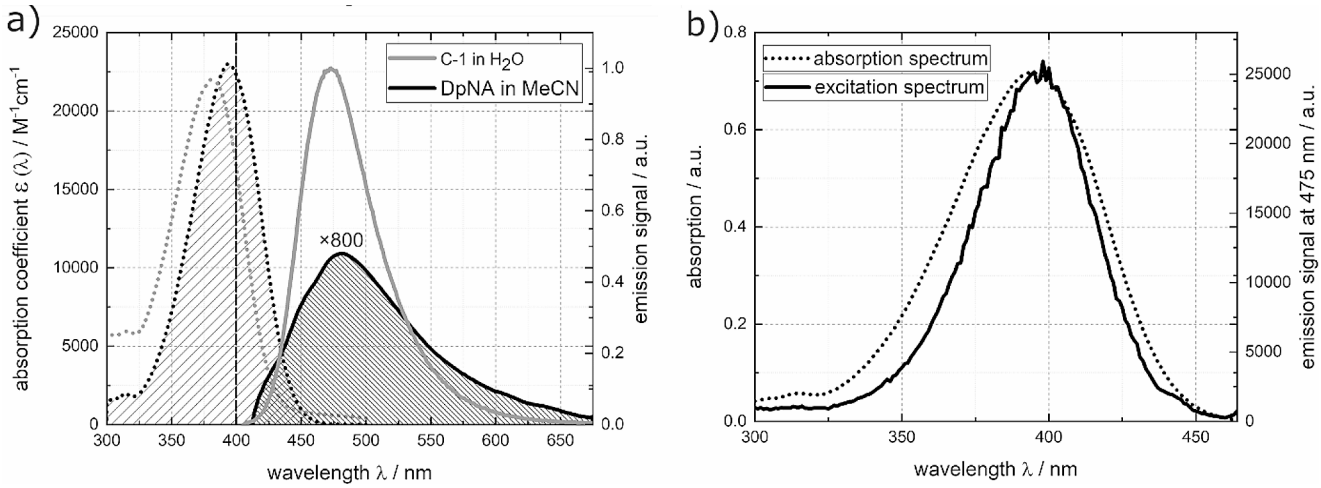

Fig. 2 (**a**) Absorption (coefficient, black dotted line) and fluorescence (smoothed black solid line) spectra of DpNA in acetonitrile. Absorption (coefficient, gray dotted line scaled according to ref. [65]) and fluorescence (gray solid line) spectra of the reference dye C-1 in water are included. The excitation wavelength at 400 nm is marked in the absorption spectra. The emission spectra were recorded with constant wavelength bandpass (5 nm). The fluorescence spectra are scaled such that their integrals are proportional to their respective fluorescence quantum yields. For the sake of comparison, the fluorescence spectrum of DpNA was multiplied by a factor of 800. The relevant ranges used for the Strickler-Berg analysis are highlighted in the absorption and emission spectra. (**b**) Fluorescence excitation spectrum of DpNA in comparison with its absorption spectrum. For the excitation spectrum the signal was probed at 475 nm

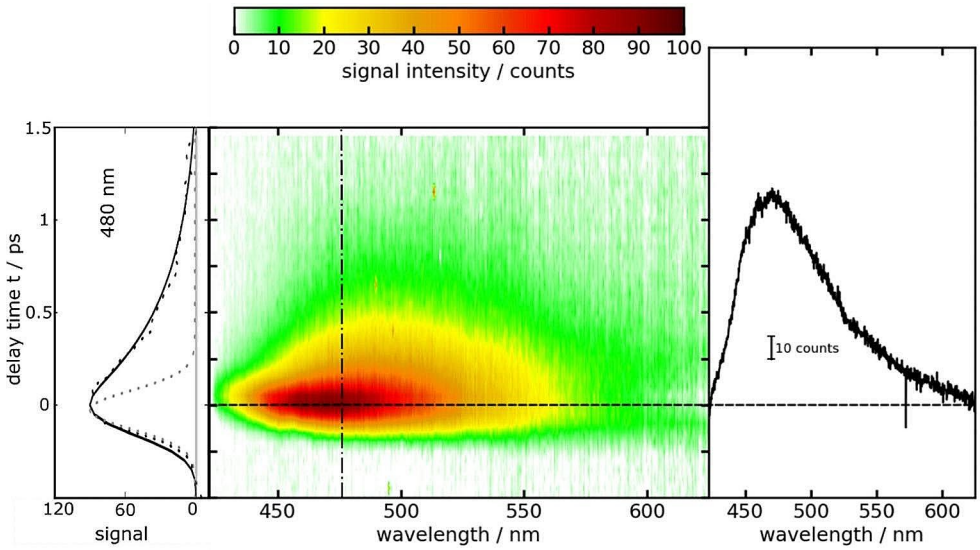

Fig. 3 Femtosecond transient fluorescence on DpNA in acetonitrile (~0.5 mM) as a function of detection wavelength λ and delay time t. The solution was excited at 400 nm. In the central contour representation, reddish hue represents large fluorescence signals. One representative time trace (480 nm) as well as a fit are shown on the left. The dotted gray line represents the IRF

decrease was observed for DpNA in acetonitrile [61]. Notably, a decrease by a factor of ~0.5 is observed. Such a non-Condon effect is not incorporated into the (standard) Strickler-Berg approach. If the reduction of the radiative rate constant k_{rad} by a factor of 0.5 is taken into account, the yields Φ_{fl}^{rel} and Φ_{fl}^{SB} match. Despite this, DpNA was discarded since for the other chromophores described below, matching values were obtained without such complications.

Blue Region of the UV/Vis Spectrum – dT in Water

The photophysics of thymidine has been extensively studied due to its fundamental role as a DNA building block [46, 67, 68]. These studies have shown that dT undergoes ultrafast internal conversion in a couple of 100 fs [69, 70]. Previous studies provide values for the fluorescence quantum yield of dT in the order of 10^{-4} [45, 46]. In this study, we aimed to reproduce these reported values. dT in water exhibits a structureless absorption band lowest in transition energy peaking around 267 nm (see Fig. 4). The fluorescence spectrum peaks at 330 nm. The spectra converted into the transition dipole representation reveal an approximate mirror-image relationship (see Fig. S2 in the Online Resource). The fluorescence excitation spectrum overlays favorably with the properly scaled absorption spectrum (Fig. 4b). Its absorption coefficient ε_{max} was determined to

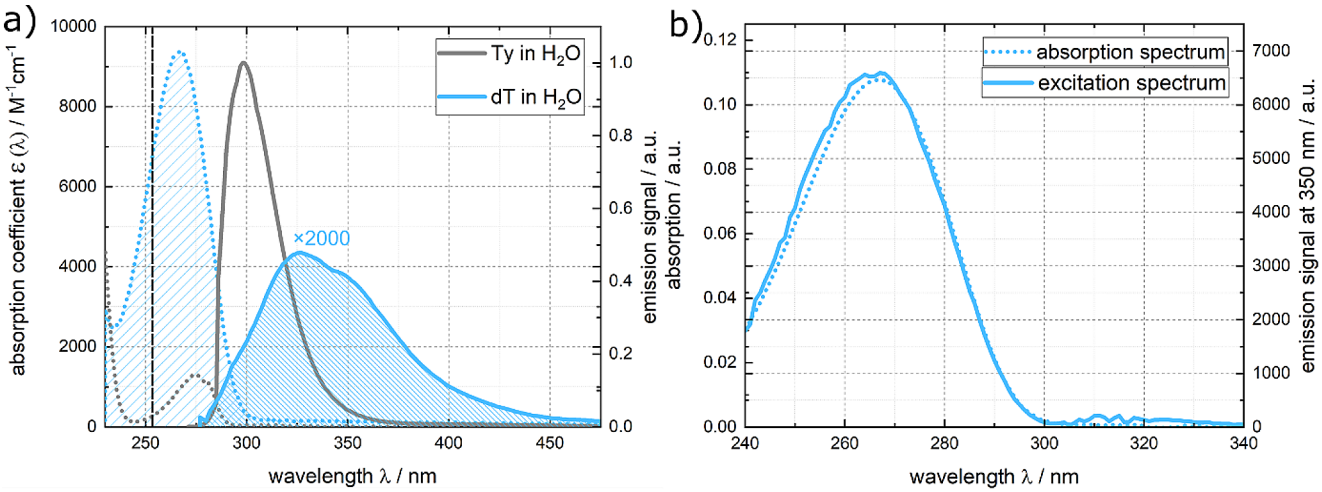

Fig. 4 (**a**) Absorption (coefficient, blue dotted line) and fluorescence (smoothed blue solid line) spectra of dT in water. Absorption (coefficient, gray dotted line scaled according to ref. [71]) and fluorescence (gray solid line) spectra of the reference dye Ty in water are included. The excitation wavelength at 255 nm is marked in the absorption spectra. The emission spectra were recorded with constant wavelength bandpass (5 nm). The fluorescence spectra are scaled such that their integrals are proportional to their respective fluorescence quantum yields. For the sake of comparison, the fluorescence spectrum of dT was multiplied by a factor of 2000. The relevant ranges used for the Strickler-Berg analysis are highlighted in the absorption and emission spectra. (**b**) Fluorescence excitation spectrum of dT in comparison with its absorption spectrum. For the excitation spectrum the signal was probed at 350 nm

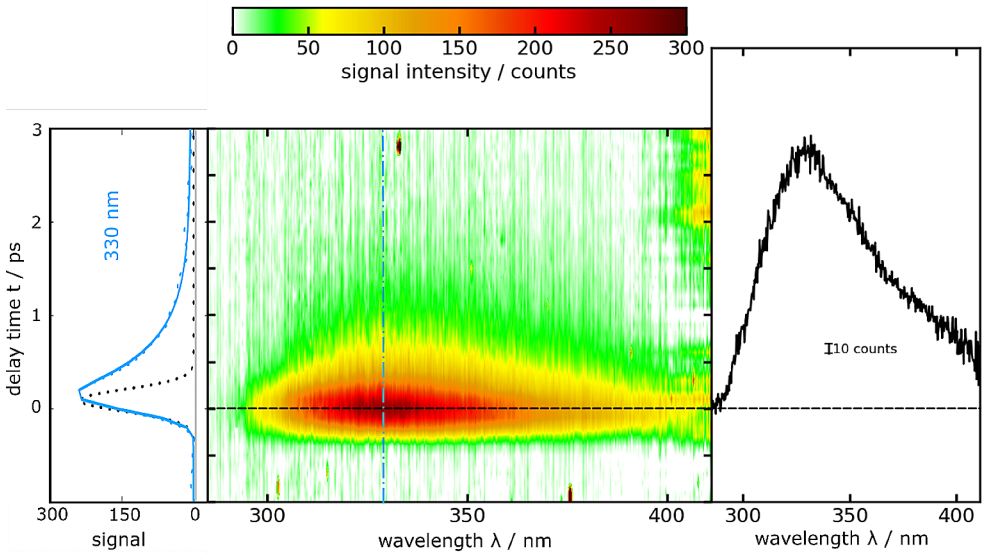

Fig. 5 Femtosecond transient fluorescence on dT in water (~1 mM) as a function of detection wavelength λ and delay time t. The solution was excited at 266 nm. In the central contour representation, reddish hue represents large fluorescence signals. One representative time trace (330 nm) as well as a single-exponential fit are shown on the left. The dotted black line represents the IRF

be $(9.4 \pm 0.1) \times 10^3$ $M^{-1}cm^{-1}$, which is somewhat smaller than the previously reported value of 9.7×10^3 $M^{-1}cm^{-1}$ [46]. For a relative determination of the fluorescence quantum yield, dT dissolved in water was excited close to the maximum at 255 nm (see Fig. 4). The resulting fluorescence signal was compared to that of Ty in water. Using Eq. (4), the relative fluorescence quantum yield Φ_{fl}^{rel} was calculated, relying on values compiled in ref. [54, 64]. From these inputs, a yield Φ_{fl}^{rel} of $(1.3 \pm 0.09) \times 10^{-4}$ for dT in water was obtained.

Using the spectra shown in Fig. 4, a Strickler-Berg analysis was performed. The relevant ranges for this analysis are highlighted in Fig. 4. This evaluation yielded a radiative rate constant k_{rad} of $(2.30 \pm 0.03) \times 10^8$ s^{-1} (see Eq. (5)).

A solution of dT in water was excited using femtosecond pulses centered at 266 nm and the resulting emission signal was probed using fluorescence Kerr gating (Fig. 5). The time resolved spectra closely resemble the shape of the steady state spectrum, exhibiting a peak around 330 nm. Within one picosecond, almost all the emission signal has vanished (Fig. 5). To determine the fluorescence lifetime $\tau_{fl.}$ of dT, a global fit of the data was performed. This analysis employed both single- and bi-exponential trial functions, convoluted with the IRF (see Experimental section). The

single-exponential fit for dT in water resulted in a fluorescence lifetime $\tau_{fl.}$ of 480 ± 140 fs. The bi-exponential fit afforded lifetimes of $\tau_1 \approx 240$ fs and $\tau_2 \approx$ 580 fs (Fig. 6). An average fluorescence lifetime $\langle \tau_{fl.} \rangle$ was derived using the Eq. (7),

$$\langle \tau_{fl} \rangle = \frac{\int DAS_1 \cdot \tau_1 + \int DAS_2 \cdot \tau_2}{\int DAS_1 + \int DAS_2}. \quad (7)$$

Here, $\int DAS_1$ and $\int DAS_2$ represent the spectral integrals of both decay associated spectra which are depicted in Fig. 6. This equation (Eq. 7) yields an average fluorescence lifetime of $\langle \tau_{fl.} \rangle = 408 \pm 190$ fs, which is somewhat smaller than the time constant obtained from the single-exponential fit. Time constants in a similar (470–700 fs) range have been reported in prior studies [46, 69, 72]. Multiplying the lifetime obtained from the single-exponential fit with the above radiative rate constant results in a fluorescence quantum yield Φ_{fl}^{SB} of $(1.11 \pm 0.3) \times 10^{-4}$ (see Eq. (2)). Inserting the average fluorescence lifetime into the same equation (Eq. 2), results in a marginally lower fluorescence quantum yield Φ_{fl}^{SB} of $(0.938 \pm 0.4) \times 10^{-4}$. However, both Φ_{fl}^{SB} values obtained here closely align with the yield Φ_{fl}^{rel} determined by the relative approach.

Green Region of the UV/Vis Spectrum – DBM in Ethanol

DBM undergoes ultrafast intramolecular proton transfer [73] upon photo-excitation. While the fluorescence quantum yield for DBM has not been quantified before, its fluorescence lifetime was found to be in the sub-picosecond range [47]. DBM in ethanol displays a structureless absorption band lowest in transition energy peaking around 340 nm (see Fig. 7). The fluorescence spectrum peaks at 400 nm. The spectra converted into the transition dipole representation reveal an approximate mirror-image relationship (see Fig. S3 in the Online Resource). The fluorescence excitation spectrum closely aligns with the properly scaled absorption spectrum for DBM in ethanol, as shown in Fig. 7b. The peak absorption coefficient ε_{max} of $(2.71 \pm 0.04) \times 10^4$ $M^{-1}cm^{-1}$ at 340 nm determined here is close to a value of 2.5×10^4 $M^{-1}cm^{-1}$ reported earlier [74]. To determine the fluorescence quantum yield of DBM relatively, a solution of DBM in ethanol was excited close to the maximum at 330 nm (see Fig. 7). The observed fluorescence signal was compared to the fluorescence of C-1 in water. Employing Eq. (4) and incorporating reference values [52, 64], the relative fluorescence quantum yield Φ_{fl}^{rel} was determined to be $(6.88 \pm 0.05) \times 10^{-5}$ for DBM in ethanol.

Utilizing the spectra presented in Fig. 7, a Strickler-Berg analysis was conducted. The relevant ranges for this analysis are highlighted in Fig. 7. From this analysis, a radiative rate constant k_{rad} of $(2.37 \pm 0.04) \times 10^8$ s^{-1} was derived (see Eq. (5)).

In the fluorescence Kerr gating experiment, femtosecond pulses centered at 266 nm were used to excite a solution of DBM dissolved in ethanol (Fig. 8). The time resolved spectra were found to closely resemble the shape of the steady state spectrum, with a peak observed around 400 nm. Within half a picosecond, nearly all the emission signal has vanished (Fig. 8). The results of the experiment were subject to a global analysis, where a single-exponential convoluted with the IRF was employed as a trial function (see Experimental Section). This analysis afforded a fluorescence lifetime $\tau_{fl.}$ of 290 ± 80 fs. A previous study reported a time constant of 240 fs [47]. By multiplying this lifetime by the radiative

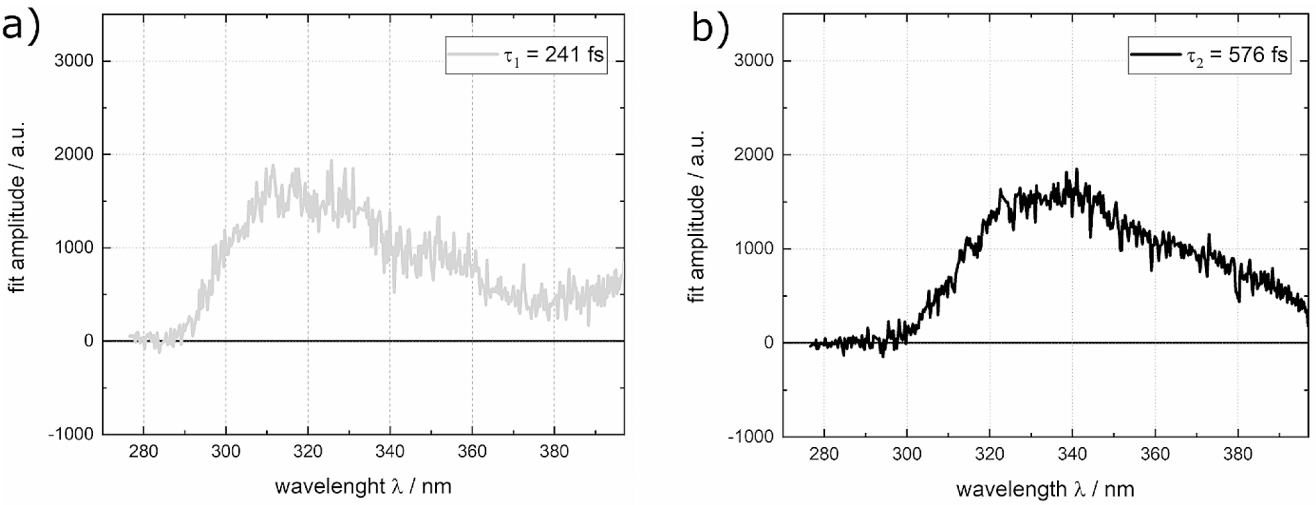

Fig. 6 Decay associated spectra (DAS) retrieved from the measurement on dT in water depicted in Fig. 5 using a bi-exponential trial function

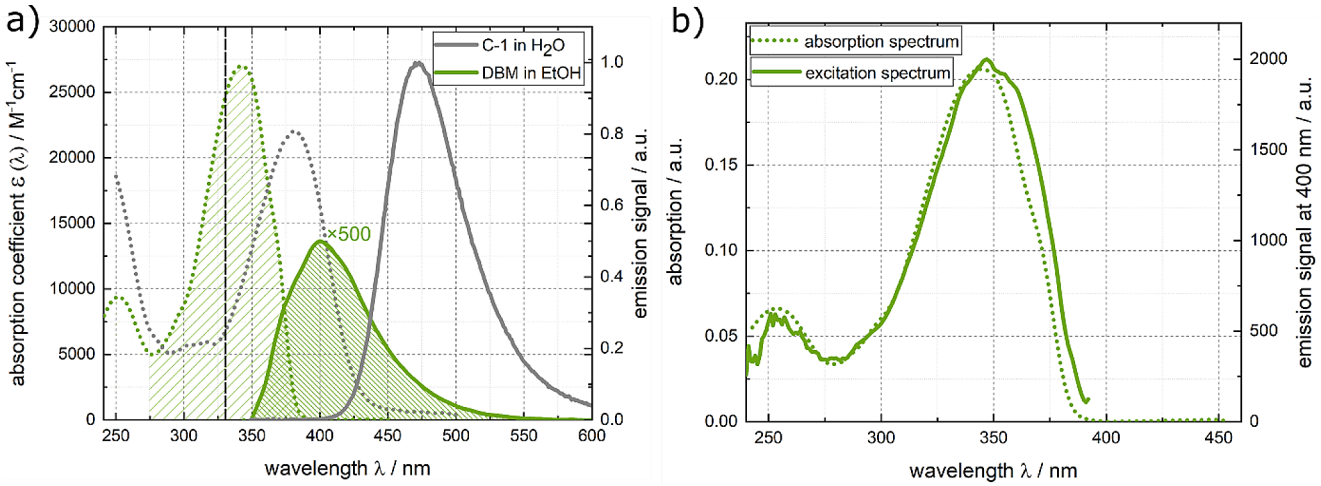

Fig. 7 (**a**) Absorption (coefficient, green dotted line) and fluorescence (smoothed green solid line) spectra of DBM in ethanol. Absorption (coefficient, gray dotted line scaled according to ref. [65]) and fluorescence (gray solid line) spectra of the reference dye C-1 in water are included. The excitation wavelength at 330 nm is marked in the absorption spectra. The emission spectra were recorded with constant wavelength bandpass (5 nm). The fluorescence spectra are scaled such that their integrals are proportional to their respective fluorescence quantum yields. For the sake of comparison, the fluorescence spectrum of DBM was multiplied by a factor of 500. The relevant ranges used for the Strickler-Berg analysis are highlighted in the absorption and emission spectra. (**b**) Fluorescence excitation spectrum of DBM in comparison with its absorption spectrum. For the excitation spectrum the signal was probed at 400 nm

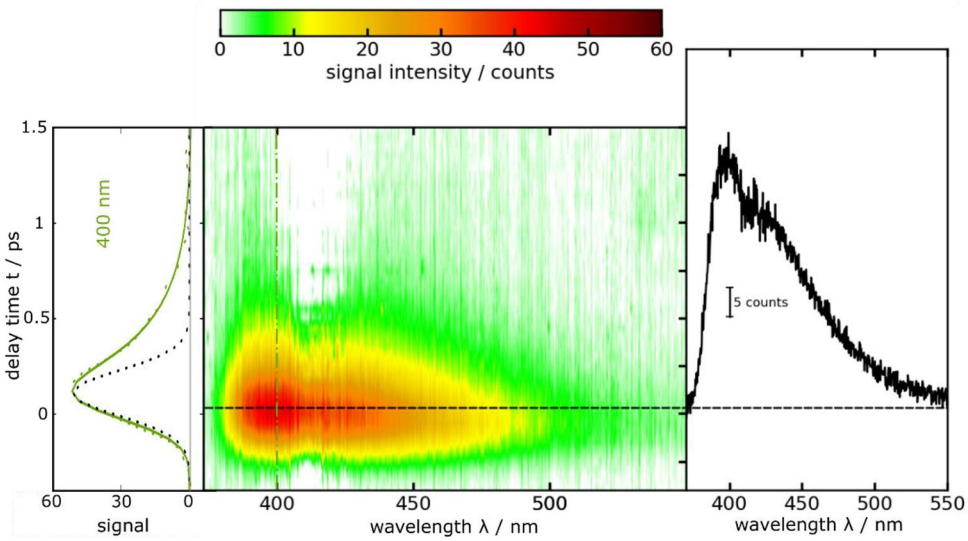

Fig. 8 Femtosecond transient fluorescence on DBM in ethanol (~ 1.3 mM) as a function of detection wavelength λ and delay time t. The solution was excited at 266 nm. In the central contour representation, reddish hue represents large fluorescence signals. One representative time trace (400 nm) as well as a fit are shown on the left. The dotted black line represents the IRF

rate constant k_{rad}, a fluorescence quantum yield Φ_{fl}^{SB} of $(6.92 \pm 1.9) \times 10^{-5}$ was calculated (see Eq. (2)).

Red Region of the UV/Vis Spectrum – MG in Water

MG, a triphenylmethane dye, exhibits pronounced visible absorption bands and has a very low fluorescence quantum yield ($\leq 10^{-4}$) in low-viscosity liquid solutions [75, 76]. Prior studies have shown that MG undergoes ultrafast internal conversion [49, 76–79]. MG in water exhibits an band lowest in transition energy peaking around 618 nm (see Fig. 9). The fluorescence spectrum peaks at 670 nm. An approximate mirror-image relationship is disclosed upon converting the spectra into the transition dipole representation (see Fig. S4 in the Online Resource). The fluorescence excitation spectrum for MG in water closely matches the properly rescaled absorption spectrum (see Fig. 9b). The peak absorption coefficient ε_{max} of $(1.43 \pm 0.01) \times 10^5$ $M^{-1}cm^{-1}$ at 618 nm determined here is in line with the value of 1.40×10^5 M^{-1} cm^{-1} reported earlier [80, 81]. For a relative determination of its fluorescence quantum yield, MG dissolved in water was excited at 535 nm (see Fig. 9). The resulting fluorescence signal was compared to the one of Rh 101 in

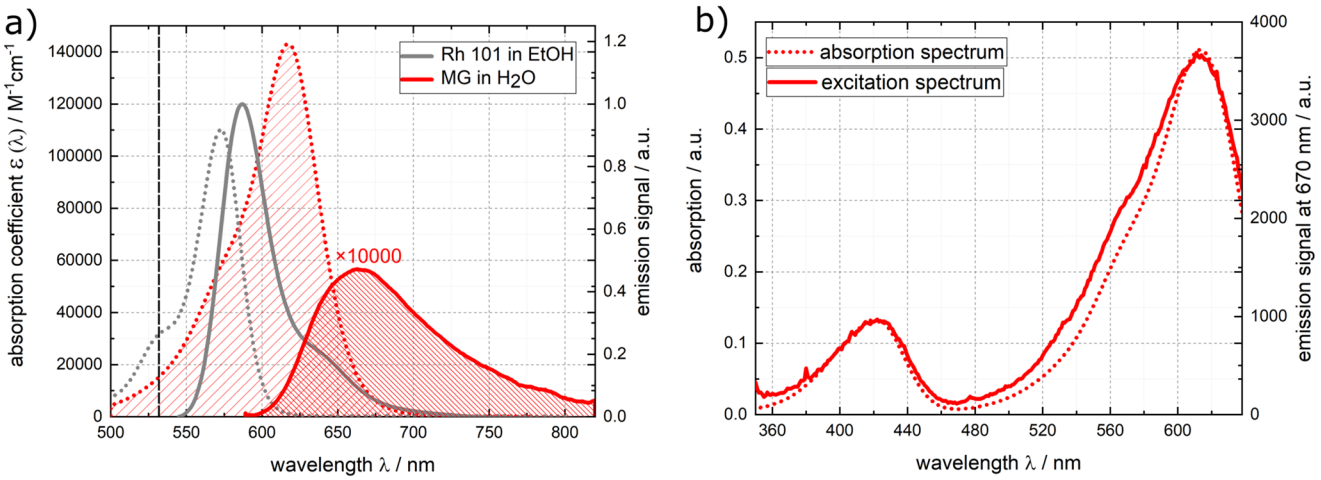

Fig. 9 (**a**) Absorption (coefficient, red dotted line) and fluorescence (smoothed red solid line) spectra of MG in water. Absorption (coefficient, gray dotted line scaled according to ref. [82]) and fluorescence (gray solid line) spectra of the reference dye Rh 101 in ethanol are included. The excitation wavelength at 535 nm is marked in the absorption spectra. The emission spectra were recorded with constant wavelength bandpass (5 nm). The fluorescence spectra are scaled such that their integrals are proportional to their respective fluorescence quantum yields. For the sake of comparison, the fluorescence spectrum of MG was multiplied by a factor of 10,000. The relevant ranges used for the Strickler-Berg analysis are highlighted in the absorption and emission spectra. (**b**) Fluorescence excitation spectrum of MG in comparison with its absorption spectrum. For the excitation spectrum the signal was probed at 670 nm

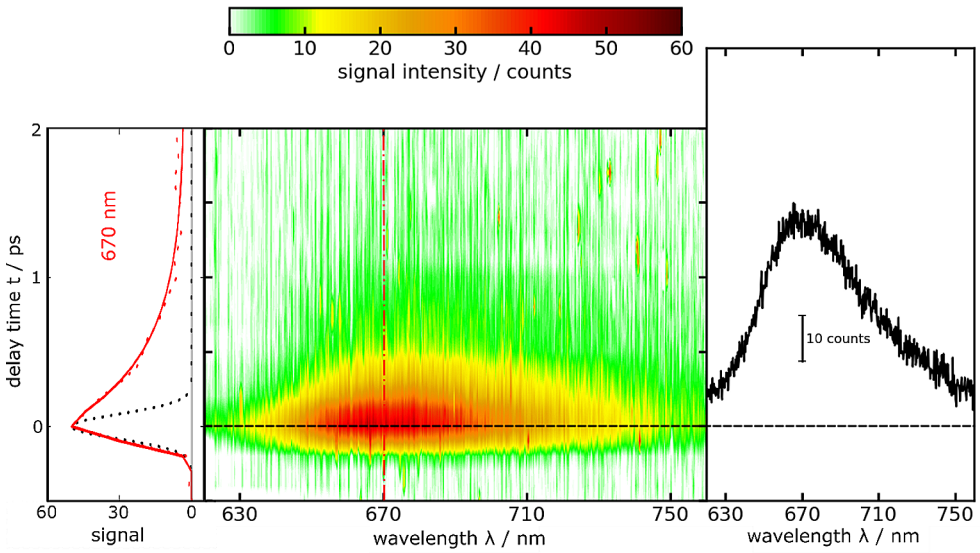

Fig. 10 Femtosecond transient fluorescence on MG in water (~ 70 µM) as a function of detection wavelength λ and delay time t. The solution was excited at 580 nm. In the central contour representation, reddish hue represents large fluorescence signals. One representative time trace (670 nm) as well as a fit are shown on the left. The dotted black line represents the IRF

ethanol. The fluorescence quantum yield based on the relative approach Φ_{fl}^{rel} was computed using Eq. (4). Values compiled in ref. [55, 64] were inserted. With these inputs, a yield Φ_{fl}^{rel} of $(9.67 \pm 0.5) \times 10^{-5}$ results for MG in water.

Using the spectra depicted in Fig. 9, a Strickler-Berg analysis was conducted. The ranges are marked in Fig. 9. The evaluation affords a radiative rate constant k_{rad} of $(2.18 \pm 0.05) \times 10^{8}$ s^{-1} (see Eq. (5)).

In the fluorescence Kerr gating experiment, femtosecond pulses with a center wavelength of 580 nm were utilized to excite a solution of MG in water (Fig. 10). The resulting time resolved spectra closely matched the steady state spectrum in shape, peaking around 670 nm. Almost the entire emission signal disappeared within one picosecond (Fig. 10). A global analysis was conducted utilizing a single-exponential function convoluted with the IRF as the trial function. This procedure yielded a fluorescence lifetime $\tau_{fl.}$ of 450 ± 160 fs. Prior studies reported time constants in a similar (520–660 fs) range [48–51]. By multiplying this lifetime by the radiative rate constant k_{rad}, a fluorescence quantum yield Φ_{fl}^{SB} of $(9.86 \pm 3.5) \times 10^{-5}$ was calculated (see Eq. (2)).

Table 1 Fluorescence quantum yields determined in this work in comparison with the earlier reports

	Φ_{fl}^{rel} from relative method	Φ_{fl}^{SB} from $k_{rad} \times \tau_{fl.}$	Φ_{fl} from prior studies
dT in water	$(1.3 \pm 0.09) \times 10^{-4}$	$(1.11 \pm 0.3) \times 10^{-4}$ [a] $(0.938 \pm 0.4) \times 10^{-4}$ [b]	1.32×10^{-4} [46], 1×10^{-4} [45]
DBM in ethanol	$(6.88 \pm 0.05) \times 10^{-5}$ [c]	$(6.92 \pm 1.9) \times 10^{-5}$	Almost non-fluorescent in solution [73, 83, 84]
MG in water	$(9.67 \pm 0.5) \times 10^{-5}$	$(9.86 \pm 3.5) \times 10^{-5}$	$< 10^{-4}$ [75], $\sim 10^{-4}$ [76]

a Based on a single-exponential fit

b Based on a bi-exponential fit

c No error margins for the yield Φ_{fl}^{r} were available

Conclusion

In this study, we propose three compounds as new references for determining small fluorescence quantum yields in the UV/Vis spectral range, with yields ranging from 10^{-5} to 10^{-4}. These compounds are thymidine in water for the blue region, dibenzoylmethane in ethanol for the green region, and malachite green chloride in water for the red region of the spectrum. Each of these compounds is easily handled, photostable, commercially available, and demonstrates a mirror-image symmetry between its absorption and fluorescence spectra. This symmetry indicates the involvement of the same electronic states in absorption and emission processes, thereby supporting the application of the Strickler-Berg relation. Furthermore, the fluorescence excitation spectra of all compounds closely align with their respective absorption spectra, confirming that the observed emissions originate from the compounds under study. The fluorescence quantum yields determined using both the relative and time resolved techniques, exhibit satisfactory agreement within their respective error margins (see Table 1). However, the error margins for the fluorescence quantum yields obtained via the time resolved technique are slightly larger, mainly due to the error in the fluorescence lifetimes (Table 1). Our findings for the fluorescence quantum yield of dT, obtained through both methods, align well with previous studies, suggesting the reliability of our results for the other compounds. It is worth noting that no value for DBM and only an upper boundary for the yield $\Phi_{fl.}$ of MG were reported previously. Here, the fluorescence quantum yields for both compounds were precisely determined.

Supplementary Information The online version contains supplementary material available at https://doi.org/10.1007/s10895-024-03729-2.

Author Contributions Mahbobeh Morshedi: sample preparation, acquisition of steady state and time resolved spectra, analysis of spectral results, computation of quantum yields, composition and editing of manuscript and figures. Simon L. Zimmermann: sample preparation, acquisition of steady state spectra, analysis of spectral results, computation of quantum yields, editing of manuscript and figures. David Klaverkamp: error analysis, editing of manuscript and figures. Peter Gilch: conceptualization, supervision, composition and editing of manuscript.

Funding This work has been supported by the Deutsche Forschungs gemeinschaft (DFG, German Research Foundation), Project number 396890929 (GRK 2482, "ModISC"). David Klaverkamp is grateful for a Kekulé scholarship from the Fonds der Chemischen Industrie. Open Access funding enabled and organized by Projekt DEAL.

Data Availability The datasets generated during and/or analysed during the current study are available from the corresponding author on reasonable request.

Declarations

Ethical Approval Not applicable.

Competing Interests The authors declare no competing interests.

References

1. Wong K-L, Bünzli J-CG, Tanner PA (2020) Quantum yield and brightness. J Lumin 224:117256. https://doi.org/10.1016/j.jlumin.2020.117256
2. Braslavsky SE (2007) Glossary of terms used in photochemistry, (IUPAC recommendations 2006). Pure Appl Chem 79:293–465. https://doi.org/10.1351/pac200779030293
3. Birriel JJ, King D (2018) Fluorescence spectra of highlighter inks. Phys Teach 56:20–23. https://doi.org/10.1119/1.5018682
4. Hoinka NM, Fuhrmann-Lieker T (2019) Amplified spontaneous emission in paper. Sci Rep 9:1862. https://doi.org/10.1038/s41598-018-38438-x

5. Kalyani NT, Dhoble S (2012) Organic light emitting diodes: Energy saving lighting technology—A review. Renew Sustain Energy Rev 16:2696–2723. https://doi.org/10.1016/j.rser.2012.02.021
6. Bauri J, Choudhary RB, Mandal G (2021) Recent advances in efficient emissive materials-based OLED applications: a review. J Mater Sci 1–30. https://doi.org/10.1007/s10853-021-06503-y
7. Suzuki T, Matsuzaki T, Hagiwara H, Aoki T, Takata K (2007) Recent advances in fluorescent labeling techniques for fluorescence microscopy. Acta Histochem Cytochem 40:131–137. https://doi.org/10.1267/ahc.07023
8. Lakowicz J (2006) In principles of fluorescence spectroscopy. Springer, Boston
9. Montalti M, Credi A, Prodi L, Gandolfi MT (2006) Handbook of photochemistry. CRC
10. Stryer L (1978) Fluorescence energy transfer as a spectroscopic ruler. Annu Rev Biochem 47:819–846. https://doi.org/10.1146/annurev.bi.47.070178.004131
11. Lerner E, Cordes T, Ingargiola A, Alhadid Y, Chung S, Michalet X, Weiss S (2018) Toward dynamic structural biology: two decades of single-molecule Förster resonance energy transfer. Science 359:eaan1133. https://doi.org/10.1126/science.aan1133
12. Mardelli M, Olmsted J III (1977) Calorimetric determination of the 9, 10-diphenyl-anthracene fluorescence quantum yield. J Photochem 7:277–285. https://doi.org/10.1016/0047-2670(77)85005-3
13. Olmsted J (1979) Calorimetric determinations of absolute fluorescence quantum yields. J Phys Chem 83:2581–2584. https://doi.org/10.1021/j100483a006
14. Gaigalas AK, Wang L (2008) Measurement of the fluorescence quantum yield using a spectrometer with an integrating sphere detector. J Res Natl Inst Stand Technol 113:17. https://doi.org/10.6028/jres.113.004
15. Würth C, Lochmann C, Spieles M, Pauli J, Hoffmann K, Schüttrigkeit T, Franzl T, Resch-Genger U (2010) Evaluation of a commercial integrating sphere setup for the determination of absolute photoluminescence quantum yields of dilute dye solutions. Appl Spectrosc 64:733–741. https://doi.org/10.1366/000370210791666390
16. Würth C, Grabolle M, Pauli J, Spieles M, Resch-Genger U (2013) Relative and absolute determination of fluorescence quantum yields of transparent samples. Nat Protoc 8:1535–1550. https://doi.org/10.1038/nprot.2013.087
17. Levitus M (2020) Tutorial: measurement of fluorescence spectra and determination of relative fluorescence quantum yields of transparent samples. Methods Appl Fluoresc 8:033001. https://doi.org/10.1088/2050-6120/ab7e10
18. Resch-Genger U, Rurack K (2013) Determination of the photoluminescence quantum yield of dilute dye solutions (IUPAC technical report). Pure Appl Chem 85. https://doi.org/10.1351/pac-rep-12-03-03
19. Cheknlyuk A, Fadeev V, Georgiev G, Kalkanjiev T, Nickolov Z (1982) Determination of fluorescence quantum yields using a spontaneous Raman scattering line of the solvent as internal standard. Spectrosc Lett 15:355–365. https://doi.org/10.1080/00387018208067999
20. Brouwer AM (2011) Standards for photoluminescence quantum yield measurements in solution (IUPAC technical report). Pure Appl Chem 83:2213–2228. https://doi.org/10.1351/PAC-REP-10-09-31
21. Klán P, Wirz J (2009) Photochemistry of organic compounds: from concepts to practice. John Wiley & Sons, UK
22. Niu Y, Peng Q, Deng C, Gao X, Shuai Z (2010) Theory of excited state decays and optical spectra: application to polyatomic molecules. J Phys Chem A 114:7817–7831. https://doi.org/10.1021/jp101568f
23. Etinski M, Tatchen J, Marian CM (2011) Time-dependent approaches for the calculation of intersystem crossing rates. J Chem Phys 134. https://doi.org/10.1063/1.3575582
24. Penfold TJ, Gindensperger E, Daniel C, Marian CM (2018) Spin-vibronic mechanism for intersystem crossing. Chem Rev 118:6975–7025. https://doi.org/10.1021/acs.chemrev.7b00617
25. Marian CM (2021) Understanding and controlling intersystem crossing in molecules. Annu Rev Phys Chem 72:617–640. https://doi.org/10.1146/annurev-physchem-061020-053433
26. Scholes GD (2003) Long-range resonance energy transfer in molecular systems. Annu Rev Phys Chem 54:57–87. https://doi.org/10.1146/annurev.physchem.54.011002.103746
27. Turro NJ, Ramamurthy V, Scaiano JC (2010) Modern molecular photochemistry of organic molecules. University Science Books, Sausalito
28. Kumpulainen T, Lang B, Rosspeintner A, Vauthey E (2017) Ultrafast elementary photochemical processes of organic molecules in liquid solution. Chem Rev 117:10826–10939. https://doi.org/10.1021/acs.chemrev.6b00491
29. Nitzan A (2006) Chemical dynamics in condensed phases: relaxation, transfer and reactions in condensed molecular systems. Oxford University Press, Oxford
30. Schrader B (2008) Infrared and Raman spectroscopy: methods and applications. Wiley, UK
31. Gustavsson T, Markovitsi D (2021) Fundamentals of the intrinsic DNA fluorescence. Acc Chem Res 54:1226–1235. https://doi.org/10.1021/acs.accounts.0c00603
32. Fujino T, Arzhantsev SY, Tahara T (2001) Femtosecond time-resolved fluorescence study of photoisomerization of trans-azobenzene. J Phys Chem A 105:8123–8129. https://doi.org/10.1021/jp0110713
33. Sajadi M, Dobryakov A, Garbin E, Ernsting N, Kovalenko S (2010) Time-resolved fluorescence spectra of cis-stilbene in hexane and acetonitrile. Chem Phys Lett 489:44–47. https://doi.org/10.1016/j.cplett.2010.02.034
34. Kochendoerfer GG, Mathies RA (1996) Spontaneous emission study of the femtosecond isomerization dynamics of rhodopsin. J Phys Chem 100:14526–14532. https://doi.org/10.1021/jp960509
35. Heinz B, Schmidt B, Root C, Satzger H, Milota F, Fierz B, Kiefhaber T, Zinth W, Gilch P (2006) On the unusual fluorescence properties of xanthone in water. PCCP 8:3432–3439. https://doi.org/10.1039/B603560D
36. Mundt R, Villnow T, Ziegenbein CT, Gilch P, Marian C, Rai-Constapel V (2016) Thioxanthone in apolar solvents: ultrafast internal conversion precedes fast intersystem crossing. PCCP 18:6637–6647. https://doi.org/10.1039/C5CP06849E
37. Rurack K (2008) Fluorescence quantum yields: methods of determination and standards. In: Resch-Genger U (ed) Standardization and Quality Assurance in fluorescence measurements I: techniques. Springer, Berlin, pp 101–145
38. Resch-Genger U, DeRose PC (2010) Fluorescence standards: Classification, terminology, and recommendations on their selection, use, and production (IUPAC Technical Report). Pure Appl Chem 82:2315–2335. https://doi.org/10.1351/PAC-REP-09-09-02
39. Resch-Genger U, Hoffmann K, Nietfeld W, Engel A, Neukammer Ja, Nitschke R, Ebert B, Macdonald R (2005) How to improve quality assurance in fluorometry: fluorescence-inherent sources of error and suited fluorescence standards. J Fluoresc 15:337–362. https://doi.org/10.1007/s10895-005-2630-3
40. Strickler S, Berg RA (1962) Relationship between absorption intensity and fluorescence lifetime of molecules. J Chem Phys 37:814–822. https://doi.org/10.1063/1.1733166
41. Parson WW (2007) Modern optical spectroscopy. Springer, Berlin

42. Mustroph H (2016) Potential-energy surfaces, the Born–Oppenheimer approximations, and the Franck–Condon principle: back to the roots. ChemPhysChem 17:2616–2629. https://doi.org/10.1002/cphc.201600243
43. Schmidt B, Laimgruber S, Zinth W, Gilch P (2003) A broadband Kerr shutter for femtosecond fluorescence spectroscopy. Appl Phys B 76:809–814. https://doi.org/10.1007/s00340-003-1230-7
44. Ciesielska B, Łukaszewicz A, Celewicz L, Maciejewski A, Kubicki J (2007) Method of determination of emission properties of very weakly emitting species ensuring elimination of emission of impurities. Appl Spectrosc 61:102–109. https://doi.org/10.1366/000370207779701389
45. Callis PR (1983) Electronic states and luminescence of nucleic acid systems. Annu Rev Phys Chem 34:329–357. https://doi.org/10.1146/annurev.pc.34.100183.001553
46. Onidas D, Markovitsi D, Marguet S, Sharonov A, Gustavsson T (2002) Fluorescence properties of DNA nucleosides and nucleotides: a refined steady-state and femtosecond investigation. J Phys Chem B 106:11367–11374. https://doi.org/10.1021/jp026063g
47. Stanimirov SS, Trifonov AA, Buchvarov IC (2021) Discovering of the L ligand impact on luminescence enhancement of Eu(dibenzoylmethane)$_3$. L_x complexes employing transient absorption spectroscopy. Spectrochim Acta Part Mol Biomol Spectrosc 258:119832. https://doi.org/10.1016/j.saa.2021.119832
48. Nagasawa Y, Ando Y, Okada T (1999) Solvent dependence of ultrafast ground state recovery of the triphenylmethane dyes, brilliant green and malachite green. Chem Phys Lett 312:161–168. https://doi.org/10.1016/S0009-2614(99)00901-X
49. Yoshizawa M, Suzuki K, Kubo A, Saikan S (1998) Femtosecond study of S_2 fluorescence in malachite green in solutions. Chem Phys Lett 290:43–48. https://doi.org/10.1016/S0009-2614(98)00483-7
50. Rafiq S, Yadav R, Sen P (2010) Microviscosity inside a nanocavity: a femtosecond fluorescence up-conversion study of malachite green. J Phys Chem B 114:13988–13994. https://doi.org/10.1021/jp1037238
51. Toyo A, Sugihara K, Nagasawa Y (2021) Nonradiative decay and vibrational dephasing of malachite green in trehalose glass monitored by femtosecond time-resolved transient absorption spectroscopy. Cryobiol Cryotechnol 67:115–119. https://doi.org/10.20585/cryobolcryotechnol.67.2_115
52. Jones G, Jackson WR, Choi CY, Bergmark WR (1985) Solvent effects on emission yield and lifetime for coumarin laser dyes. Requirements for a rotatory decay mechanism. J Phys Chem 89:294–300. https://doi.org/10.1021/j100248a024
53. White A (1959) Effect of pH on fluorescence of tyrosine, tryptophan and related compounds. Biochem J 71:217. https://doi.org/10.1042/bj0710217
54. Teale F, Weber G (1957) Ultraviolet fluorescence of the aromatic amino acids. Biochem J 65:476. https://doi.org/10.1042/bj0650476
55. Rurack K, Spieles M (2011) Fluorescence quantum yields of a series of red and near-infrared dyes emitting at 600–1000 nm. Anal Chem 83:1232–1242. https://doi.org/10.1021/ac101329h
56. Satzger H, Zinth W (2003) Visualization of transient absorption dynamics–towards a qualitative view of complex reaction kinetics. Chem Phys 295:287–295. https://doi.org/10.1016/j.chemphys.2003.08.012
57. van Stokkum IH, Larsen DS, Van Grondelle R (2004) Global and target analysis of time-resolved spectra. Biochim et Biophys Acta -Bioenergetics 1657:82–104. https://doi.org/10.1016/j.bbabio.2004.04.011
58. Bevington PR, Robinson DK, Blair JM, Mallinckrodt AJ, McKay S (1993) Data reduction and error analysis for the physical sciences. Computers Phys 7:415–416. https://doi.org/10.1119/1.17439
59. Beechem JM, Gratton E, Ameloot M, Knutson JR, Brand L (2002) Top fluorescence spectroscopy: principles 241–305. https://doi.org/10.1007/0-306-47058-6_5. The global analysis of fluorescence intensity and anisotropy decay data: second-generation theory and programs
60. Thomsen C, Thøgersen J, Keiding S (1998) Ultrafast charge-transfer dynamics: studies of p-nitroaniline in water and dioxane. J Phys Chem A 102:1062–1067. https://doi.org/10.1021/jp972492g
61. Kovalenko S, Schanz R, Hennig H, Ernsting N (2001) Cooling dynamics of an optically excited molecular probe in solution from femtosecond broadband transient absorption spectroscopy. J Chem Phys 115:3256–3273. https://doi.org/10.1063/1.1380696
62. Angulo G, Grampp G, Rosspeintner A (2006) Recalling the appropriate representation of electronic spectra. Spectrochimica Acta Part A: Mol Biomol Spectrosc 65:727–731. https://doi.org/10.1016/j.saa.2006.01.007
63. Al-Yasari A, Van Steerteghem N, Kearns H, El Moll H, Faulds K, Wright JA, Brunschwig BS, Clays K, Fielden J (2017) Organoimido-polyoxometalate nonlinear optical chromophores: a structural, spectroscopic, and computational study. Inorg Chem 56:10181–10194. https://doi.org/10.1021/acs.inorgchem.7b00708
64. Kozma IZ, Krok P, Riedle E (2005) Direct measurement of the group-velocity mismatch and derivation of the refractive-index dispersion for a variety of solvents in the ultraviolet. JOSA B 22:1479–1485. https://doi.org/10.1364/JOSAB.22.001479
65. Baleeva NS, Zaitseva SO, Mineev KS, Khavroshechkina AV, Zagudaylova MB, Baranov MS (2019) Enamine–azide [2+3]-cycloaddition as a method to introduce functional groups into fluorescent dyes. Tetrahedron Lett 60:456–459. https://doi.org/10.1016/j.tetlet.2019.01.007
66. Farztdinov VM, Schanz R, Kovalenko SA, Ernsting NP (2000) Relaxation of optically excited p-nitroaniline: Semiempirical quantum-chemical calculations compared to femtosecond experimental results. J Phys Chem A 104:11486–11496. https://doi.org/10.1021/jp001690w
67. Middleton CT, de La Harpe K, Su C, Law YK, Crespo-Hernández CE, Kohler B (2009) DNA excited-state dynamics: from single bases to the double helix. Annu Rev Phys Chem 60:217–239. https://doi.org/10.1146/annurev.physchem.59.032607.093719
68. Gustavsson T, Improta R, Markovitsi D (2010) DNA/RNA: building blocks of life under UV irradiation. J Phys Chem Lett 1:2025–2030. https://doi.org/10.1021/jz1004973
69. Pecourt J-ML, Peon J, Kohler B (2001) DNA excited-state dynamics: Ultrafast internal conversion and vibrational cooling in a series of nucleosides. J Am Chem Soc 123:10370–10378. https://doi.org/10.1021/ja0161453
70. Crespo-Hernández CE, Cohen B, Hare PM, Kohler B (2004) Ultrafast excited-state dynamics in nucleic acids. Chem Rev 104:1977–2020. https://doi.org/10.1021/cr0206770
71. Scappini F, Casadei F, Zamboni R, Monti S, Giorgianni P, Capobianco M (2007) Laboratory simulation of UV irradiation from the Sun on amino acids. I: irradiation of tyrosine. Int J Astrobiol 6:123–129. https://doi.org/10.1017/S1473550407003588
72. Peon J, Zewail AH (2001) DNA/RNA nucleotides and nucleosides: direct measurement of excited-state lifetimes by femtosecond fluorescence up-conversion. Chem Phys Lett 348:255–262. https://doi.org/10.1016/S0009-2614(01)01128-9
73. Verma PK, Koch F, Steinbacher A, Nuernberger P, Brixner T (2014) Ultrafast UV-induced photoisomerization of intramolecularly H-bonded symmetric β-diketones. J Am Chem Soc 136:14981–14989. https://doi.org/10.1021/ja508059p
74. Zawadiak J, Mrzyczek M (2014) Super-strong bathochromic and hyperchromic effects of methoxy-substituted aromatic

bis (1,3-diketones). Mendeleev Commun 1:45–46. https://doi.org/10.1016/j.mencom.2013.12.015
75. Ippen EP, Shank C, Bergman A (1976) Picosecond recovery dynamics of malachite green. Chem Phys Lett 38:611–614. https://doi.org/10.1016/0009-2614(76)80053-X
76. Zhou Y, Gurzadyan GG, Ni W, Gelin MF, Sun L (2020) Upper excited state photophysics of malachite green in solution and films. J Phys Chem B 124:4293–4302. https://doi.org/10.1021/acs.jpcb.0c01737
77. Abedin KM, Ye JY, Inouye H, Hattori T, Sumi H, Nakatsuka H (1995) Diffusive torsional dynamics of malachite green molecules in solid matrices probed by fluorescence decay. J Chem Phys 103:6414–6425. https://doi.org/10.1063/1.470420
78. Laptenok SP, Addison K, Heisler IA, Meech SR (2014) Excited state structural dynamics in higher lying electronic states: S2 state of malachite green. Chem Phys Lett 607:43–46. https://doi.org/10.1016/j.cplett.2014.05.050
79. Bhasikuttan AC, Sapre AV, Okada T (2003) Ultrafast relaxation dynamics from the S_2 state of malachite green studied with femtosecond upconversion spectroscopy. J Phys Chem A 107:3030–3035. https://doi.org/10.1021/jp034486s
80. Nakashima K, Duhamel J, Winnik M (1993) Photophysical processes on a latex surface: electronic energy transfer from rhodamine dyes to malachite green. J Phys Chem 97:10702–10707. https://doi.org/10.1021/j100143a029
81. Maxwell EJ, Tong WG (2016) Sensitive detection of malachite green and crystal violet by nonlinear laser wave mixing and capillary electrophoresis. J Chromatogr B 1020:29–35. https://doi.org/10.1016/j.jchromb.2016.02.040
82. Beija M, Afonso CA, Martinho JM (2009) Synthesis and applications of rhodamine derivatives as fluorescent probes. Chem Soc Rev 38:2410–2433. https://doi.org/10.1039/B901612K
83. Tobita S, Ohba J, Nakagawa K, Shizuka H (1995) Recovery mechanism of the reaction intermediate produced by photoinduced cleavage of the intramolecular hydrogen bond of dibenzoylmethane. J Photochem Photobiol Chem 92:61–67. https://doi.org/10.1016/1010-6030(95)04158-X
84. Zhang G, Evans RE, Campbell KA, Fraser CL (2009) Role of boron in the polymer chemistry and photophysical properties of difluoroboron–dibenzoylmethane polylactide. Macromolecules 42:8627–8633. https://doi.org/10.1021/ma9019043